

Modeling the micro-indentation of metal matrix composites

M.R. Rosenberger^{a,c,*}, E. Forlerer^b, C.E. Schvezov^c

^a CONICET (Consejo Nacional de Investigaciones Científicas y Técnicas), Rivadavia 1917, (1033) Buenos Aires, Argentina

^b Departamento de Materiales, Centro Atómico Constituyentes, CNEA, Av. Gral. Paz 1499, (1650) San Martín, Argentina

^c Prog. Materiales, Modelización y Metrología, FCEQyN, Universidad Nacional de Misiones, Azara 1552, (3300) Posadas, Misiones, Argentina

Received 20 March 2006; received in revised form 18 September 2006; accepted 18 September 2006

Abstract

A finite element model is developed to quantify the effect of the depth and diameter of the reinforcement in the hardness number of metal matrix composite. The model includes a spherical indenter pressed against a metal containing one reinforcing particle. The results are validated for the non-reinforced material comparing the results of the simulation with analytical models that calculate the properties of the material using Brinell and Meyer hardness and the load–displacement curve. A simple composite consisting of a ductile matrix containing one hard particle of size 0.25–1 of the indenter size and placed at depths 0.1–0.5 times the indenter radius are assumed. The diameters and depths of the impressions for reinforced and matrix materials are determined for different particle size and positions, and the influence on the hardness number is calculated. An overestimation in hardness of reinforced materials was observed with the values dependant on the position and size of the particle. Maximum overestimations of 15% using visual inspection and of 74% using the Oliver and Pharr technique were found in the reinforced materials. In addition, if the impression diameter is at least twice the diameter of the reinforcement, a maximum error of 5% in hardness is produced.

© 2006 Elsevier B.V. All rights reserved.

Keywords: Microhardness; Modeling; Metal matrix composite; Finite elements method; Indentation

1. Introduction

Microhardness test is a commonly used technique to determine mechanical properties of materials during fabrication of metallic parts [1–5]. In the case of metal matrix composite (MMC) containing hard particles as reinforcements, the scatter in hardness measurements could be as large as 20% [6–10]. In order to explain this large scatter several approaches have been employed, such as analytical models of strengthening of the composite materials [11–15] and numerical models for matrix strengthening, load transfer and models that apply a combination of both [13,15].

The models of matrix strengthening include various mechanisms, which consider the particle/matrix interfaces, a high concentration of dislocation near the interfaces, the internal stress in the matrix, and accelerated precipitation kinetics as strengthening factors [11]. The models of load transfer assume

that hard and rigid reinforcements are able to hold, transmit and distribute the load in the matrix, focusing on the transfer of load by the particle/matrix interface. It has been reported that the load transfer models may apply for volume fractions lower than 20% [13,16] whereas the matrix strengthening models may apply in the case of reinforcement smaller than 1 μm [17].

1.1. Modeling of hardness test

Several theoretical, experimental and modeling studies have been reported which seek to understand the variation in impression hardness [18–25]. In all cases the main objective was [3,26] to find a relation between hardness measurement and macroscopic properties such as elastic module and yield strength. That relation may be employed on the characterization of small samples, coatings, thin films, individual phases in alloys and composite materials, strain hardening and residual stress.

The classical methods used to measure hardness employ the load to application area ratio. The determination of the application area is performed by the measurement of a characteristic length such as the impression depth, impression diameter; or

* Corresponding author. Tel.: +54 3752 427491; fax: +54 3752 425414.
E-mail addresses: rrmario@fceqyn.unam.edu.ar (M.R. Rosenberger), forlerer@cnea.gov.ar (E. Forlerer), Schvezov@fceqyn.unam.edu.ar (C.E. Schvezov).

Nomenclature

BH	Brinell hardness
d_L	impression depth at maximum load
d_{p_i}	initial particle depth
d_{p_L}	particle depth at maximum load
d_{p_U}	particle depth after unloading
d_U	impression depth after unloading
h	generic depth
K	constant of proportionality
MH	Meyer hardness
MMC	metal matrix composite
n	strain hardening exponent
P	load
r	impression radius
r_L	impression radius at maximum load
r_p	particle radius
r_U	impression radius after unloading
R_i	indenter radius
z_L	vertical displacement of the impression border at maximum load
z_U	vertical displacement of the impression border after unloading
<i>Greek letters</i>	
ε	strain
σ	stress
σ_s	yield strength

the difference between minimum to maximum indenter depth. There are two forms of calculating the application area; one, considers the total area of the impression and another, considers the projected area of the impression [23,26,27]. In both cases, the measurement of the characteristic length may be affected by the plastic deformation of the surface produced during the indentation process.

More modern methods employ indentation machines, which continually record the applied force versus the displacement of the indenter. Several forms were proposed to calculate the hardness from the analysis of the plot load versus displacement [20,23,28]. One of these methods proposed by Oliver and Pharr [28] is widely used to calculate the hardness [3,29]. It employs the region of plot where the indenter is withdrawing and it is based in general assumptions on the elastic recovering of the tested material to calculate the hardness number and the elastic modulus. The Oliver and Pharr method was originally developed to quantify the nanohardness of the bulk of metals and ceramics [28], and it is presently employed to quantify the hardness of other materials like polymers [3], composites materials [29,30] and thin films [31], some reports are indicating that this technique has a limited capacity to measure the hardness of soft films on a hard substrate [31], and some composite materials [29].

The plastic deformation of the surface around the impression can produce an error in the measured characteristic length

used to calculate the hardness number. This deformation may occur near the border of the impression in two modes; *sinking in* or *piling up* [20,23,27,31–34]. Both have a notable influence on the diameter and depth of the impression, and therefore on the hardness number used for the calculation of Brinell, Meyer, Rockwell or Vickers hardness numbers.

In the case of particle or fiber MMC the studies can be classified in two groups; one in which the impression covers both the matrix and the reinforcements [35–39] and the other which employs a microhardness approach where the hardness of the matrix and reinforcement are determined separately [2,4,5,29,30,40,41]. The main conclusion of these studies is that the hardness measurements overestimate both the yield and the ultimate strengths [5,37–40].

The overestimation of the results is attributed to the observation of an increase in the density of particles by the indenter [38,39]. The influence of the reinforcing particles close to the impression on the hardness measurements has been discussed in the literature [5,29], and as a result a recommendation has been proposed for performing indentation away from visible particles for more than three times the size of the indentation; results of this procedure are conservative since it has been showed that the effect of the particles is negligible when they are separated by a distance of two times the size of the indentation [29]. However, when the particle is not visible in the sample surface the effect may not be noted unless the measured hardness is far from the average value.

In the present work the influence of the size and depth of subsurface particles on hardness is studied employing computational modeling. Macroscopic properties were assumed and microscopic mechanisms of matrix strengthening were neglected. The model assumes a weak particle/matrix interface when the load transfer is driven by friction forces according to the Coulomb law (or Amonton law), which assumes that the friction force is linearly proportional to the normal force applied between the two surfaces in contact, and independent of the superficial area and the relative velocity. The coefficient of proportionality is known as the friction coefficient.

The model is built using the finite element method and was validated with experimental values and analytical models of hardness for non-reinforced materials.

2. Methods

2.1. Description of the system

The system is modeled with a semi-infinite ductile matrix, which contains one spherical particle as reinforcement buried in the subsurface, and a semi-spherical tip indenter placed over the surface of the matrix. The line connecting the particle and the tip indenter centers intercepts the surface at a right angle, as shown in Fig. 1.

The load is applied monotonically on the indenter achieving the maximum value in 30 s; after this the indenter is withdrawn.

An impression to indenter radius ratio of 0.521 for the non-reinforced material was assumed in the study, which is a typical value for a Brinell hardness test in aluminum alloy [42].

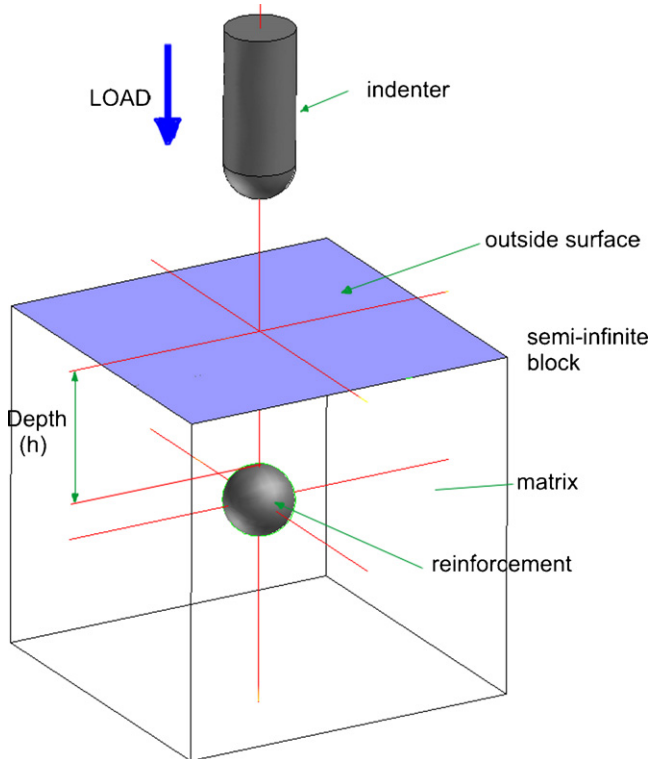


Fig. 1. Domain of the system employed in the model.

The particle to indenter size ratios (r_p/R_i) used in this study are: 0.25, 0.3, 0.5, 0.6, 0.8 and 1. The particle depth to indenter radius ratios (d_p/R_i) are: 0.1, 0.2, 0.3, 0.4, 0.5, and infinite; other ratios are added to obtain a detailed description of the process around critical points.

Macroscopic properties and no length scales were assumed, therefore no “size effect” or bias of the hardness number with the size of the impression [4,43,44] is contemplated in the model. These assumptions neglect microscopic strengthening in the matrix, focusing on the load transfer model. One indenter radius (R_i) was employed for the whole study.

2.2. Mathematical model

In order to apply an in-house code of finite element method for a quasi-steady process the whole axi-symmetric domain was meshed, with remeshing after each time step to avoid element distortion. The meshed domain includes the indenter, the particle and a volume of matrix material assumed to be a cylinder of 50–200 times the particle volume.

About 30,000 toroidal elements of quadrilateral sections and first order interpolation functions are employed in the mesh. A non-structured mesh spread the whole domain, with a larger density of nodes placed near the contact boundaries with elements as small as $0.004 R_i$, as shown in Fig. 2.

The finite element code was developed using the Galerkin method to solve the energy balance. The contact between different components of the domain was treated using the augmented Lagrangian multiplier method and the Coulomb friction model,

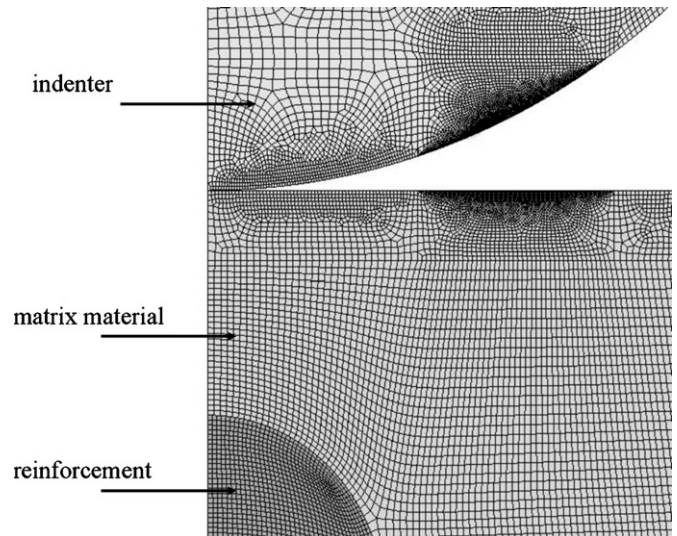


Fig. 2. Detail of the mesh employed containing toroidal elements with quadrilateral section.

the friction forces are incorporated numerically by the penalty method [45–47].

The following assumptions were made:

- The elastic deformation of the matrix and the particle are linear.
- The plastic deformation follows the Von Mises criterion with isotropic matrix hardening.
- The system is isothermal.
- The system geometry is axi-symmetric.

The time analysis is performed by an implicit method with a variable time step, in the interval of 10^{-7} to 0.1 s with a modal value of 0.001 s. The system of equations is solved by the Newton–Raphson method [48–50]. A tolerance of 10^{-3} is employed for the relative global error by iteration.

2.3. Initial and boundary conditions

No displacement in the vertical direction is assumed on a horizontal plane located 0.05 m from the top of the matrix.

The load applied to the indenter is perpendicular to the surface of the matrix, and gradually increases from zero to the maximum load in 30 s, after this the indenter is withdrawn.

Whitehead [51] has reported a value of friction coefficient of around 1.25 measured between aluminum and steel for loads between 10^{-4} and 10^2 N, in the present model a friction coefficient of one is imposed at the particle/matrix interface.

A non-perfect bonded interface between matrix and reinforced is assumed as opposed to a perfect contact which corresponds to an infinite value of the friction coefficient, the other limit is zero for a frictionless interface. A value of 1 is a good assumption, which is consistent with the value employed for the indenter/matrix interface. Other authors [1] have employed values smaller and closer to zero.

The matrix material is assumed to be an aluminum alloy, the indenter material is steel and the reinforcing particles are

Table 1
Materials properties [42,52]

Property	Aluminum alloy	Steel	SiC
Density (kg/m ³)	2700	7800	3210
Elastic module (GPa)	70	200	400
Yield strength (MPa)	215	700	–
Traction strength, ϵ (MPa)	250 (0.20)	830 (0.20)	–
Poisson module	0.33	0.287	0.19

assumed to be silicon carbide, the values of the mechanical parameters employed are listed in Table 1 [42,52] and are assumed to be constant.

3. Results and discussion

3.1. Model validation

The model has been validated for aluminum alloy employing the radius of impressions obtained with the model to estimate the hardness and then the yield strength (σ_s). For the model calculations an indenter 10 mm in diameter was assumed and a load of 14,709 N was applied. The diameter of the impressions obtained was 5.208 mm, which corresponds to Meyer hardness (MH) of 690.5 MN/m², calculated as [23]

$$MH = \frac{P}{\pi r^2} \quad (1)$$

where P is load, and r is the impression radius; and a Brinell hardness (BH) of 652.4 MN/m². From the last value and employing the following relation [19,27]:

$$BH \approx 3\sigma_s \quad (2)$$

a value for σ_s of 217.5 MN/m² is obtained, which is very similar to the value of 215 MN/m² used in the model, showing a very good consistency.

In addition, the model is validated in the plastic region as follows: the shear stress–strain relation for the plastic deformation employed in the model is

$$\sigma = K\epsilon^n \quad (3)$$

assuming a strain hardening exponent (n) of 0.033 which is compared with the same index calculated with the model. In the last case the load to impression depth (P – h) curve resulting from the model and the relation between P and h [23]

$$P \propto h^{1+(n/2)} \quad (4)$$

are used to fit the P – h curve obtained with the simulation and shown in Fig. 3. The result is an exponent n of 0.03, which is again within 10% of the input value showing also good consistency.

Moreover, using the relation proposed by Tabor [19,27], the σ_s value can be estimated using the following relation:

$$MH \approx 3\sigma_s \left(\frac{0.2r}{R_i} \right)^n \quad (5)$$

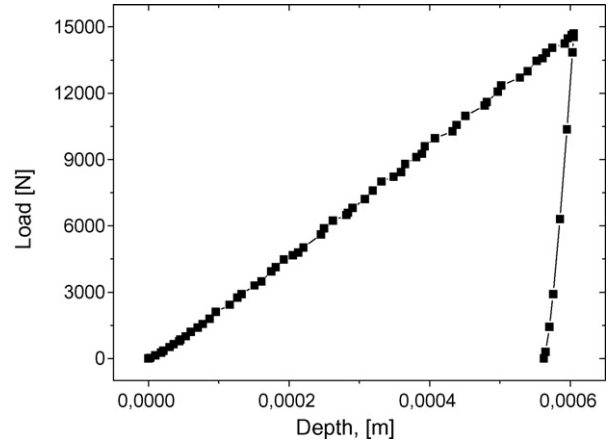


Fig. 3. Plot of load vs. depth (P – h), of the non-reinforced material.

where R_i is the indenter radius and assuming n equal to 0.03. The resulting value of σ_s is 247.9 MN/m² which is slightly higher than that used as model input.

3.2. Results for the MMCs

Fig. 4 shows the scheme of the impression profiles observed in the load and unload conditions which were obtained as a result of the simulations. The dimensions employed in the analysis are explained in nomenclature.

The radius of the impression is determined by the farthest point from the indenter central axis in the testing material which is in contact with the indenter at the highest load, marked as A in Fig. 4. After the indenter was withdrawn the point A moves to A' and this position is registered as the unload radius of the impression.

The depth of the impression is taken as the distance traveled by the indenter from the initial position, $z=0$, to the full load position, see Fig. 4.

The displacements of the reinforcement in the loaded and unloaded conditions are registered as the direct measures of the

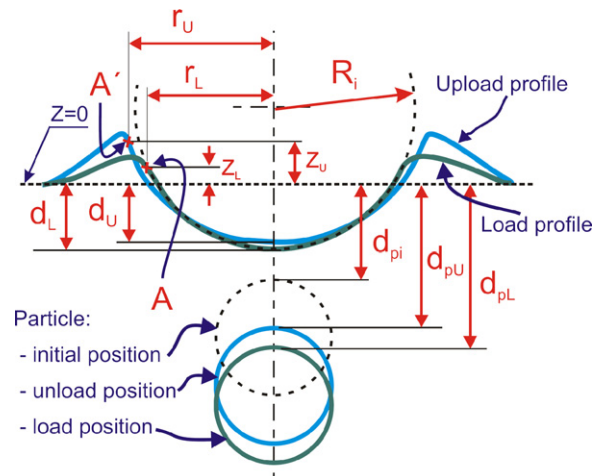


Fig. 4. Schematic representation of the impression profiles results of the simulations and the different parameters used in the text, and defined in nomenclature.

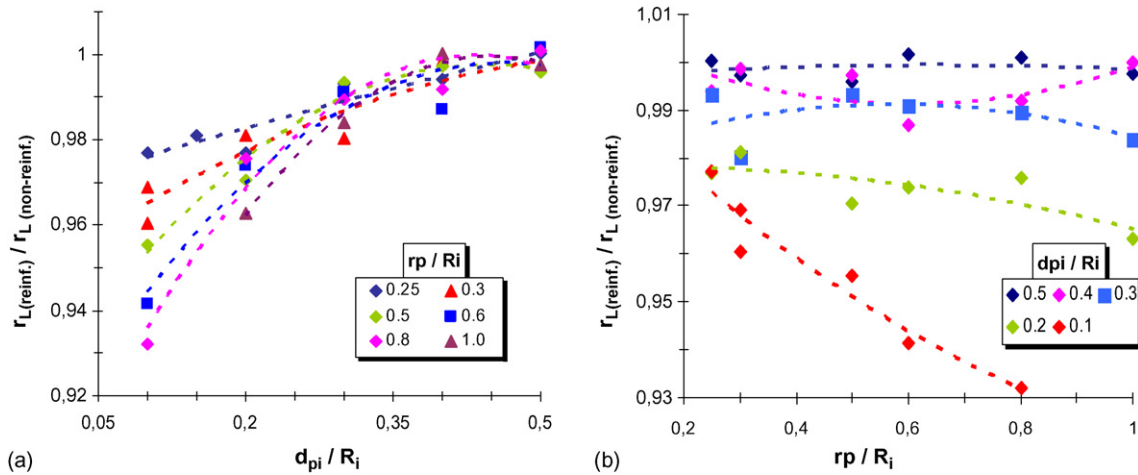


Fig. 5. Relative impression radius of the reinforced materials at maximum load, (a) as a function of relative particle depth for different relative particle radii; (b) as a function of relative particle radius for different relative particle depths.

displacement of the top point of the particle surface, with respect to its initial position in each condition, see Fig. 4.

The results were normalized relative to the values of the same parameters under the same modeling conditions obtained for aluminum alloy. In addition, both; the reinforcing particle depth and radius are scaled to the radius of the indenter.

In Fig. 5(a) the normalized diameter of the impression in the load condition is represented as a function of the depth of the reinforcing particle also in non-dimensional values for different particle radius.

In Fig. 5(a) it is observed that all the diameters of the impressions are less than one and that the value tends to one as the depth of the particle increases, that is; the impression tends to a diameter equal to that of a non-reinforced material. This behavior holds for all particle sizes. On the other hand, for low particle depths the diameter of the impression decreases as the particle size increases.

In Fig. 5(b) the impression radius is represented as a function of particle radius for different particle depths. It is observed that

the most pronounced effect of particle radius on the impression is for the shallowest particle ($d_{pi} / R_i = 0.1$) and the effect is less pronounced as the particle depth increases; for relative depths larger than 0.4 the effect of particle radius is negligible.

The difference in diameter between the loaded and unloaded impressions is a way of characterizing the degree of elastic recovery after indentation. This parameter is plotted in Fig. 6, relative to the same difference obtained for aluminum alloy under the same testing conditions, as a function of the non-dimensional particle depth in Fig. 6(a), and particle radius in Fig. 6(b). In Fig. 6(a) the elastic recovery is presented for different non-dimensional particle radius and it is shown that the recovery is always less than one with a stronger dependence on particle depth as the relative particle radius increases. For small particles of radius less than 0.3 the effect is negligible, however in all cases, as the depth tends to infinity the elastic recovery tends to one, as expected. The complementary representation in Fig. 6(b) shows this strong dependence on particle radius for all particle depths. In addition, in all cases as the particle radius tends to

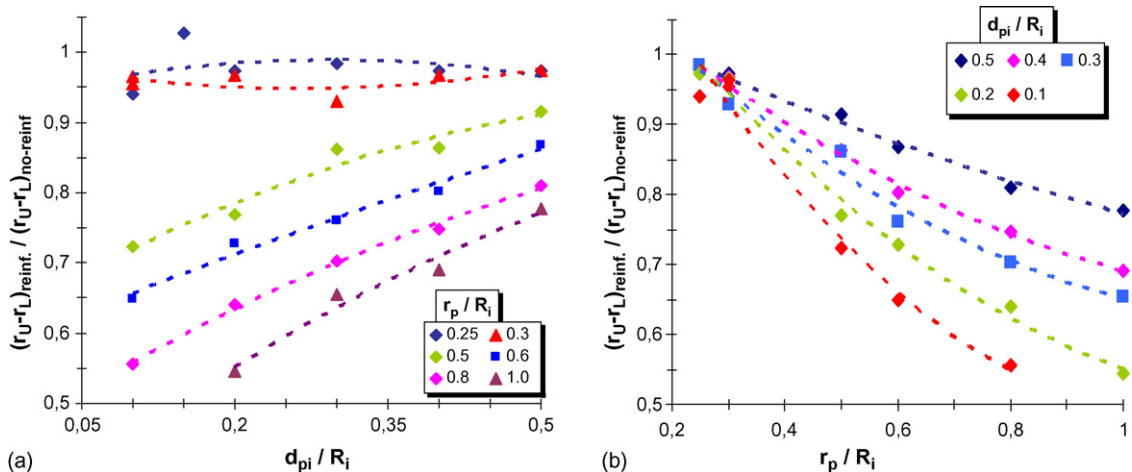


Fig. 6. Elastic recovery of the impression, (a) as a function of relative particle depth for different relative particle radii; (b) as a function of relative particle radius for different relative particle depths.

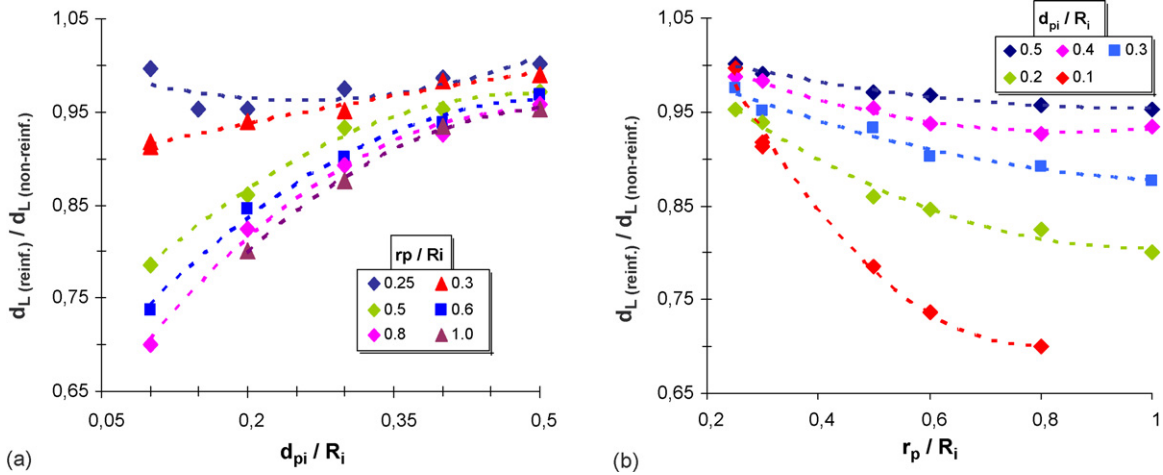


Fig. 7. Relative impression depth, (a) as a function of relative particle depth for different relative particle radii; (b) as a function of relative particle radius for different relative particle depths.

zero the recovery tends to one very rapidly with a slight non-linearity as compared with the effect of particle radius which is linear. The elastic recovery of the impression in the unload position is not uniform as it is usually assumed in the literature but it is asymmetric; producing a reduction in the depth of the impression by elevation of the bottom and a consequent enlargement of the impression border, as can be observed in Fig. 4.

The non-dimensional depth of the impression in the loaded position as function of particle depth and particle radius is shown in Fig. 7(a) and (b), respectively; in Fig. 7(a) for different particle depths and in Fig. 7(b) for different particle radius. In both figures it is observed that in all cases the depth is always less than one, showing that the impressions in the reinforced material are shallower than in the pure matrix. In both figures the behavior is similar to that observed with the previous parameters, that is; a larger effect for shallower particles and also for larger reinforcements. Fig. 7(a) shows the negligible effect of particle depth on the impression depth for particles of relative size less than 0.25. However, what is clear and different in the behavior of impression depth shown here, is the stronger non-linearity with respect

to particle depth and radius. In each case the slope increases as the depth and radius decrease.

3.3. Effect of reinforcement on hardness number

The Meyer hardness number of the composite materials obtained with the model results are presented in Fig. 8. The numbers are relative values with respect to the number corresponding to the matrix material under the same testing conditions. In Fig. 8(a) and (b) the hardness values are plotted against particle depth for different particle radius, and as function of particle radius for different particle depth. Again, these parameters are normalized relative to the indenter radius.

In Fig. 8(a) it is observed as before, that the hardness increases as the depth decreases, which for shallow particles is as high as 15% of the hardness of the non-reinforced material.

Using the technique proposed by Oliver and Pharr the increase in hardness of reinforced material could be as high as 74% with respect to the non-reinforced material, as it can be observed in Fig. 9. It is necessary to mention that with the proposed technique, the hardness for non-reinforced material is

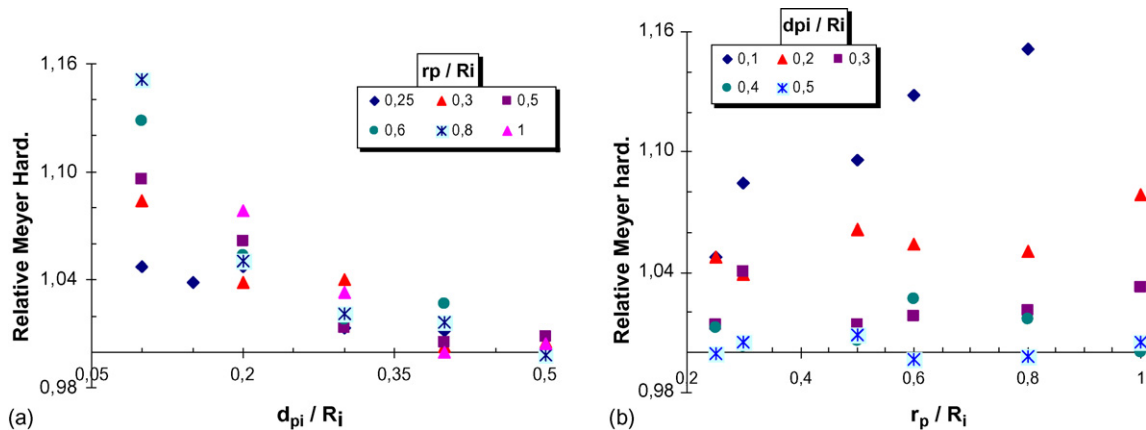


Fig. 8. Meyer hardness of the reinforced materials normalized respect to the non-reinforced material, (a) as a function of relative particle depth for different relative particle radii; (b) as a function of relative particle radius for different relative particle depths.

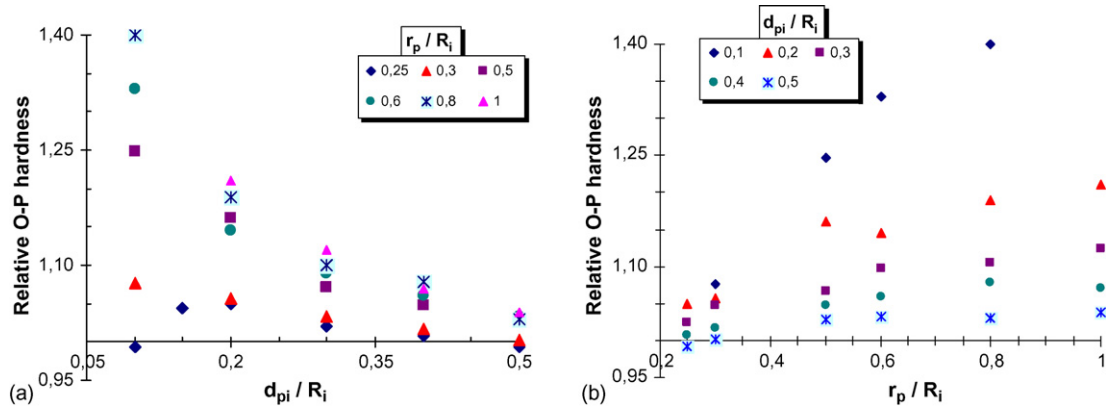


Fig. 9. Oliver and Pharr hardness of the reinforced materials normalized respect to the non-reinforced material, (a) as a function of relative particle depth for different relative particle radii; (b) as a function of relative particle radius for different relative particle depths.

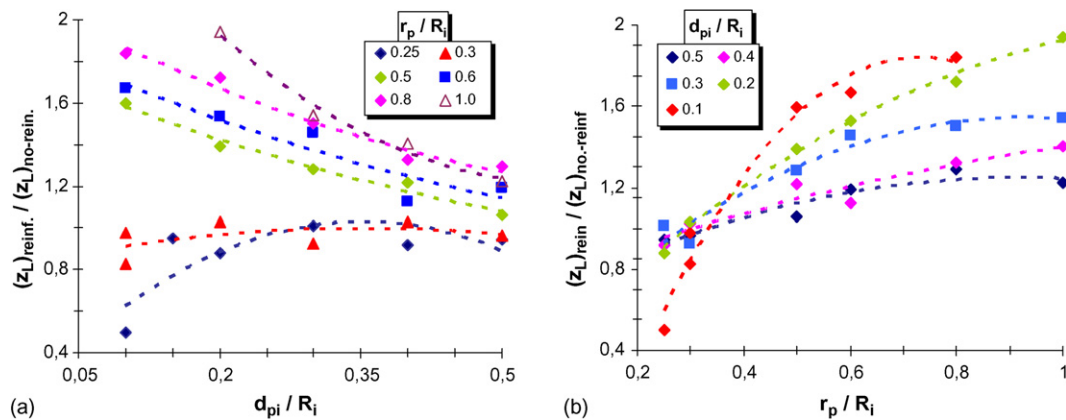


Fig. 10. Vertical displacement of the impression border at the load condition, normalized respect to the non-reinforced material, (a) as a function of relative particle depth for different relative particle radii; (b) as a function of relative particle radius for different relative particle depths.

1.24 times higher than that obtained by direct observation of the impression diameter.

In order to establish the factors leading to this large overestimation, the flow of material due to the indentation process is analyzed. An indicative of the magnitude of the flow is given by the upward displacement of the impression borders. This quantity is represented in Fig. 10(a) and (b) as functions of particle depth and particle radius, respectively. In Fig. 10(a) it is observed that for particle radius larger than 0.5 the flow is larger than for the non-reinforced matrix material and that the amount of the flow is larger as the depth decreases. The effect of shallow particles is clearly observed in Fig. 10(b) for depth of 0.2 and 0.1 where the displacement is twice the amount corresponding to the non-reinforced matrix materials. This result is indicating that when the particles are larger and shallower they are more able to support the applied load by the indenter.

This reasonable assumption is confirmed by the results shown in Fig. 11. In the figure the downward displacement of the reinforcing particle due to indentation is represented as a function of particle radius for different particle depths. The downward displacement is given as the relation between the final depth divided by the initial depth. The first observation is that all the curves for the different particle depths converge to one as the relative particle radius converges to one, that is, when the particle and the

indenter size is the same, the indenter is not displaced by the particle during indentation. On the other hand, as the particle radius decreases the particle displacement increases with a more pronounced dependence for shallower particles. In summary, larger and shallower particles are not displaced from their initial position, supporting the indenter load, and producing more flow of

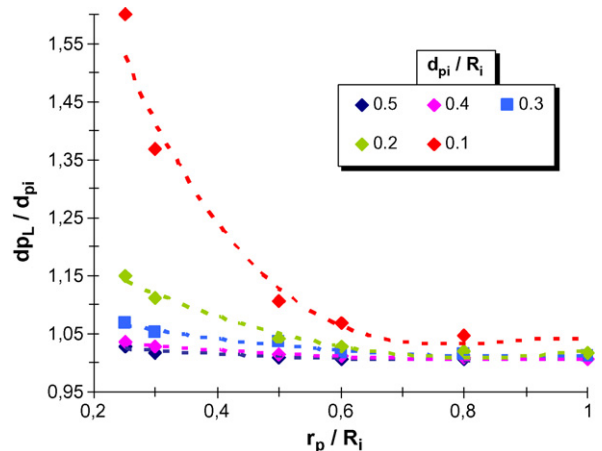


Fig. 11. Sinking of the reinforcement, final depth to initial depth ratio, as a function of the relative particle radius.

matrix material with the result of more prominent impression borders.

The pile-up of material in the surface of the impression border can cause discrepancies in the hardness readings such as those obtained with the Oliver and Pharr technique which does not account for the displacement of material towards the surface or pile-up [26,34].

In summary, the results reported here indicate an important effect of the presence of reinforcement in the hardness measurements. For a ductile matrix containing a particle in the subsurface an overestimation of obtained of about 15% in the hardness number is obtained if the impression diameter is determined visually. In the case of an indentation process carried out by an automatic instrument using the procedure proposed by Oliver and Pharr, the overestimation could be as high as 74% due to the presence of a particle, which act as a hard substrate increasing the pile up at the surface.

These observations and the modeling conditions applied for the indentation process indicate the convenience of employing impressions with size at least twice the size of the reinforced particles which give acceptable errors of 5% in the measurements, in either case; visual determination or instrumented indentation. In all cases to obtain reasonable values, the particle depth should be more than 0.2 times the impression diameter. Otherwise the obtained results should be carefully considered.

4. Conclusions

The effect of reinforcement depth and size of hard particles in a MMC on microhardness measurement was studied using numerical modeling. The particle radius ranged from 0.25 to 1 times the radius of the indenter, and an impression radius 0.5 times the indenter radius. A summary of the significant findings based on the modeling results include:

1. The hardness measurements may be overestimated by 15–74% depending on the method employed, visual inspection or the Oliver and Pharr method [28], respectively.
2. The ideal measurement configuration is that in which the impression diameter is at least twice the diameter of the reinforcement, giving a maximum error of 5%.
3. Large and shallow particles are not displaced by the indenter under the modeling conditions and result in a larger flow of material in the matrix material between particle and surface. The ability to support the load is directly related to the particle size and inversely related to particle depth.
4. The larger flow of material in the above case produces a higher elevation of the impression border, which influence the diameter and depth of the impression and results in incorrect hardness measures.

References

- [1] M. Drissi-Habti, K. Nakano, J. Eur. Ceram. Soc. 18 (1998) 1845–1855.
- [2] M. Drissi-Habti, K. Nakano, K. Suzuki, Compos. Part A 30 (1999) 471–475.
- [3] M.R. Van Landingham, J. Res. Natl. Inst. Stand. Technol. 108 (2003) 249–265.
- [4] O. Yoldas, T. Akova, H. Uysal, Polym. Test 23 (3) (2004) 343–346.
- [5] E.R. Olivas, J.G. Swadener, Y.-L. Shen, Scripta Mater. 54 (2006) 263–268.
- [6] J. Zhang, A.T. Alpas, Mater. Sci. Eng. A 160 (1993) 25–35.
- [7] B. Venkataraman, G. Sundararajan, Acta Mater. 44 (2) (1996) 461–473.
- [8] H.C. How, T.N. Baker, Wear 232 (1999) 106–115.
- [9] K.A. Khor, Y.W. Gu, D. Pan, P. Cheang, Biomaterials 25 (2004) 4009–4017.
- [10] M.R. Rosenberger, E. Forlerer, C.E. Schvezov, Wear 259 (1–6) (2005) 590–601.
- [11] T. Christman, A. Needleman, S. Suresh, Acta Metall. 37 (1989) 3029–3050.
- [12] Y. Wu, E.J. Lavernia, Scripta Metall. Mater. 27 (1992) 173–178.
- [13] R.M. Aikin Jr., J. Metals 49 (8) (1997) 35–39.
- [14] Z. Jiang, G. Li, J. Lian, X. Ding, J. Sun, Compos. Sci. Tech. 64 (2004) 1661–1670.
- [15] M. Mondali, A. Abedian, S. Adibnazari, Comput. Mater. Sci. 34 (2005) 140–150.
- [16] C. Cayron, Thesis of Doctorado no. 2246, Escuela Politecnica Federal de Lausanne, Lausanne, Francia, 2000.
- [17] J. Rosler, Mater. Sci. Eng. A 339 (2003) 334–339.
- [18] Y. Tirupataiah, G. Sundararajan, Metall. Trans. A 22 (1991) 2375–2384.
- [19] D. Tabor, Phil. Mag. A 74 (5) (1996) 1207–1212.
- [20] A.E. Giannakopoulos, S. Suresh, Scripta. Mater. 40 (10) (1999) 1191–1198.
- [21] Y.-T. Cheng, C.-M. Cheng, Int. J. Solids Struct. 36 (1999) 1231–1243.
- [22] Y.-T. Cheng, C.-M. Cheng, Surf. Coat. Tech. 133–134 (2000) 417–424.
- [23] J. Alcala, A.C. Barone, M. Anglada, Acta Mater. 48 (13) (2000) 3451–3464.
- [24] H. Pelletier, J. Krier, A. Cornet, P. Mille, Thin Solid Films 379 (2000) 147–155.
- [25] S. Kucharski, Z. Mroz, Mater. Sci. Eng. A 318 (2001) 65–76.
- [26] Y.-T. Cheng, C.-M. Cheng, Mater. Sci. Eng. R 44 (2004) 91–149.
- [27] D. Tabor, Hardness of Metals, Clarendon Press, Oxford, 1951.
- [28] W.C. Oliver, G.M. Pharr, J. Mater. Res. 7 (6) (1992) 1564–1580.
- [29] J.L. Bucaille, A. Rossoll, B. Moser, S. Stauss, J. Michler, Mater. Sci. Eng. A 369 (2004) 82–92.
- [30] K.M. Mussert, W.P. Vellinga, A. Bakker, S. Van Der Zwaag, J. Mater. Sci. 37 (4) (2002) 789–794.
- [31] X. Chen, J.J. Vlassak, J. Mater. Res. 16 (10) (2001) 2974–2982.
- [32] C. Shaw, Y. Li, H. Jones, Mater. Lett. 28 (1996) 33–36.
- [33] M.L. Weaver, M.E. Stevenson, R.C. Bradt, Mater. Sci. Eng. A 345 (2003) 113–117.
- [34] G.M. Pharr, Mater. Sci. Eng. A 253 (1998) 151–159.
- [35] H.S. Kim, M.B. Bush, Y. Estrin, Mater. Sci. Eng. A 276 (2000) 175–185.
- [36] H.S. Kim, Mater. Sci. Eng. A 289 (2000) 30–33.
- [37] S. Suresh, Science 292 (2001) 2447–2451.
- [38] Y.-L. Shen, J.J. Williams, G. Piotrowski, N. Chawla, Y.L. Guo, Acta Mater. 49 (2001) 3219–3229.
- [39] R. Pereyra, Y.-L. Shen, Mater. Charact. 53 (2004) 373–380.
- [40] M. Zidi, L. Carpentier, A. Chateauminois, F. Sidoroff, Comp. Sci. Tech. 60 (2000) 429–437.
- [41] M. Zidi, L. Carpentier, A. Chateauminois, P. Kapsa, F. Sidoroff, Comp. Sci. Tech. 61 (2001) 369–375.
- [42] H.E. Boyer, T.L. Gall (Eds.), Metals Handbook, Desk ed., ASM, Ohio, 1985.
- [43] H. Yuan, J. Chen, Comp. Mater. Sci. 25 (2002) 253–263.
- [44] K. Sangwal, Mater. Chem. Phys. 63 (2000) 145–152.
- [45] C. Agelet de Saracibar, M. Chiumenti, Comput. Meth. Appl. Mech. Eng. 177 (1999) 401–426.
- [46] N.G. Bourago, in: S.A. Ivanenki, V.A. Garanzha (Eds.), Proceedings of the International Workshop Grid Generation and Industrial Applications, Moscow, 2002, pp. 42–59.

- [47] H.L. Xing, A. Makinouchi, *Comput. Meth. Appl. Mech. Eng.* 191 (2002) 4193–4214.
- [48] T.R. Chandrupatla, A.D. Belegundu, *Introducción al Estudio Del Elemento Finito en Ingeniería*, Prentice Hall, México, 1999.
- [49] S.C. Chapra, R.P. Canale, *Numerical Methods for Engineers*, McGraw-Hill, 2002.
- [50] K.H. Huebner, E.A. Thornton, *The Finite Element Method for Engineers*, John Wiley and Sons, USA, 1982.
- [51] J.R. Whitehead, *Proc. Roy. Soc. A* 201 (1950) 109–124 (cited in E. Rabinowicz, 1995, *Friction and wear of materials*. John Wiley and Sons, USA).
- [52] MEMS Online Data base: www.memsnet.org/material/siliconcarbidesicbulk/.